Near-surface diagnostics of dripping or delaminating lithosphere

Oğuz H. Göğüş[1] and Russell N. Pysklywec[1]

[1]   In various geological regions, it has been postulated that the mantle lithosphere has been thinned or completely removed. Two of the primary removal mechanisms that have been put forward include: (1) delamination, a wholesale peeling away of a coherent block of the mantle lithosphere, and (2) lithospheric "dripping," viscous Rayleigh-Taylor instability of the mantle lithosphere. Using computational models, we investigate several near-surface observables to determine if these may be diagnostic of either (often ambiguous) removal mechanism. Surface topography associated with delamination has a broad region of uplift above the lithospheric gap and a localized and mobile zone of subsidence at the delaminating hinge. With dripping lithosphere, the topographic expression is symmetric and fixed above the downwelling. Delamination of mantle lithosphere is more efficient than dripping for thermal heating of the crust; the onset is more rapid and the elevated temperatures persist longer. The resultant crustal P-T-t paths show modest pressure variations and high temperature increases with large-scale delamination or dripping. Delamination also causes contraction directly above the (migrating) hinge and distal extension. Dripping lithosphere induces superimposed contraction and extension above and symmetric about the viscous instability. For all the observables, if only a portion of the mantle lithosphere is removed by viscous instability (delamination inherently removes all of the mantle lithosphere), the differences between the two removal mechanisms are even more pronounced. With only partial removal of the mantle lithosphere, uppermost mantle lithosphere remains well coupled to the crust, leading to lower surface temperature variations and broad zones of crustal deformation/thickening.

1.   Introduction

[2]   The removal of the mantle lithosphere (i.e., the sub-crustal portion of the lithosphere) has been invoked in a variety of tectonic regimes to account for a range of geological, geophysical and geochemical observations. For example, anomalous heating, topography, and gravity has led to interpretations that mantle lithosphere has been removed during some phase of the plate convergence at the Andean margin [*Kay and Kay*, 1993; *Beck and Zandt*, 2002], India-Eurasia collision [*Bird*, 1978; *Houseman et al.*, 1981], New Guinea collisional zone [*Cloos et al.*, 2005], and Eastern Anatolian Plateau [*Keskin*, 2003]. Within the interior of continental tectonic plates, such as at the Sierra Nevada mountains [*Ducea and Saleeby*, 1998; *Jones et al.*, 2004; *Zandt et al.*, 2004] and beneath the Colorado Plateau [*Bird*, 1979] the removal of the mantle lithosphere has been proposed to explain regional uplift. These mantle lithosphere removal events are generally based on the density contrast of the mantle lithosphere with respect to the less dense underlying mantle. The density contrast can arise as a result of thermal contraction of the cold mantle lithosphere, although compositional density variations of the lower crust have also been called upon to explain lithospheric instability [*Jull and Kelemen*, 2001; *Elkins-Tanton*, 2005].

[3]   The geodynamic mechanisms in which mantle lithosphere is removed are still debated, but there are fundamentally two primary removal scenarios that have been put forward. *Bird* [1978, 1979] proposes a model of mantle lithosphere delamination, where the cold and dense mantle lithosphere peels away as a coherent slice from the crust along the Moho. The removed slice of mantle lithosphere is replaced by hot and buoyant asthenosphere (Figure 1A). Generally, delamination is predicated on the idea that the hot-weak lower crust is the most pronounced strength discontinuity in the lithosphere. This results in separation between the strong crust and strong mantle lithosphere portions of the plate. *Morency and Doin* [2004] used 2-D numerical simulations of convection with a viscoplastic rheology to study the delamination mechanism and in particular consider the geodynamic conditions that cause this type of lithospheric removal. They suggest that delamination begins with localized thinning of the mantle lithosphere and where the highest Moho temperature is

---

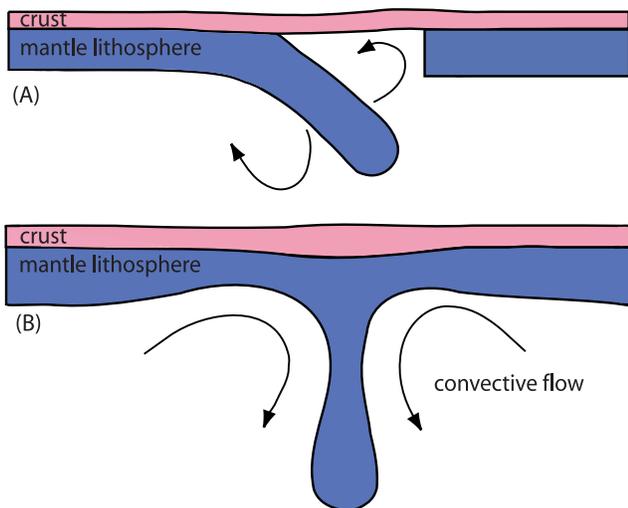[1]Department of Geology, University of Toronto, Toronto, Ontario, Canada.

Figure 1. Schematic illustration of geodynamic models for mantle lithosphere removal. (A) Delamination of the mantle lithosphere [*Bird*, 1979]. (B) Convective removal of the mantle lithosphere [*Houseman et al.*, 1981].

achieved, progressive thermomechanical erosion of lithospheric mantle occurs because of asthenospheric upwelling. This leads to sinking of the dense mantle lithosphere slice into the asthenosphere. The authors intimate that delamination is only possible when Moho temperatures exceed approximately 800°C.

[4] Delamination has been associated with topographic and thermal perturbation of the crust. It is suggested that regional uplift of the Sierra Nevadas, Andes, and Colorado plateau has developed through mantle lithosphere delamination events in these areas [*Bird*, 1979; *Jones et al.*, 2004; *Le Pourhiet et al.*, 2006]. Uplift is largely the result of isostatic adjustment from replacing dense mantle lithosphere with buoyant asthenosphere, although flexure and deformation of the plate also cause topographic variations [*Le Pourhiet et al.*, 2006]. The nature of delamination means that hot asthenosphere comes into direct contact with the crust. The presence of high potassium intrusives and high crustal heat flow has been put forward as the thermal/magmatic signature of delamination [*Kay and Kay*, 1993; *Ducea and Saleeby*, 1998; *Manley et al.*, 2000].

[5] An alternative lithospheric removal mechanism to delamination is viscous convective removal of the mantle lithosphere [e.g., *Houseman et al.*, 1981; *England and Houseman*, 1989]. In this case, some or all of the mantle lithosphere may be removed as cold dense mantle lithosphere "drips" as a viscous Rayleigh-Taylor (RT) gravitational instability (Figure 1B). The primary difference from delamination is that the mantle lithosphere is not removed as a coherent lithospheric slice, but deforms in a distinctly "un-platelike" manner as it descends/drips into the mantle. Subsequent studies have demonstrated that the propensity of the lithosphere to experience convective removal is controlled by the viscous rheology of the mantle lithosphere [e.g., *Buck and Toksoz*, 1983; *Lenardic and Kaula*, 1995; *Houseman and Molnar*, 1997; *Molnar et al.*, 1998]. In addition, the timescale and character of these viscous pertur-

bations can be influenced by horizontal shortening of the lithosphere [e.g., *Conrad and Molnar*, 1997; *Molnar et al.*, 1998], and the presence of an overlying crust [e.g., *Neil and Houseman*, 1999; *Pysklywec and Cruden*, 2004]. The explicit assumption of these models is that there is sufficient perturbation (and at a suitable wavelength) to the mantle lithosphere to initiate Rayleigh-Taylor instability. Furthermore, the growth rate of the instability must outpace thermal diffusion of the cold mantle lithosphere root into the hot mantle.

[6] It is worthwhile to clarify that we use the term delamination following its definition by the process of *Bird* [1979]. We differentiate this from the viscous process of Rayleigh-Taylor instability (or "convective removal" or "dripping") of the mantle lithosphere. Often the term delamination is used to denote any type of mantle lithosphere removal event. This introduces ambiguity relating to what are quite different processes with different surface expressions, as we will demonstrate.

[7] As with delamination, the replacement of the dense mantle lithosphere by more buoyant mantle can cause isostatic surface uplift. This type of mechanism has been used to interpret the Tibetan plateau uplift [*England and Houseman*, 1989] and the anomalous regional topography across the southern Sierra Nevada [*Saleeby and Foster*, 2004]. *Neil and Houseman* [1999] demonstrate that in certain situations viscous dripping can also induce thickening of the overlying crust and hence further surface uplift. These isostatic responses are complemented by mantle flow-induced topography as the viscous dripping progresses [e.g., *Pysklywec and Shahnas*, 2003; *Pysklywec and Cruden*, 2004]. *Saleeby and Foster* [2004] suggest that the subsidence of the Tulare Lake basin, in the southern Great Valley is driven by active mantle dripping. The adjacent uplift and tilting of the Sierra Nevada range may be related to thinning of the mantle lithosphere peripheral to the drip [*Zandt et al.*, 2004].

[8] Thus, as mantle lithosphere removal mechanisms, it has been shown or postulated that both delamination and Rayleigh-Taylor instability will produce a variety of thermal and deformational responses of the crust. Consequently, in regions where removal of the mantle lithosphere seems to have taken place, such as the Sierra Nevada, as discussed above, initial interpretation of the surface constraints may lead to ambiguity about which mechanism is active.

[9] The purpose of this paper is to investigate in more detail the crustal and surface observables that may be used as diagnostic elements to differentiate between the two of mantle lithosphere removal processes: delamination or Rayleigh-Taylor-type convective removal/dripping. We designed a series of forward numerical experiments representing both types of removal mechanisms. We focus on four primary properties during evolution of the model: (1) surface topographic evolution, (2) distribution and style of crustal deformation, (3) thermal evolution of various levels within the crust, and (4) the metamorphic (P-T-t) evolution of lower, middle, and upper crust. These represent surface or near-surface observables that may generally characterize the thermal-mechanical evolution of the lithosphere during mantle lithosphere removal. Our intent is that by doing a direct comparison using generic models, the results will provide clearer quantitative information for
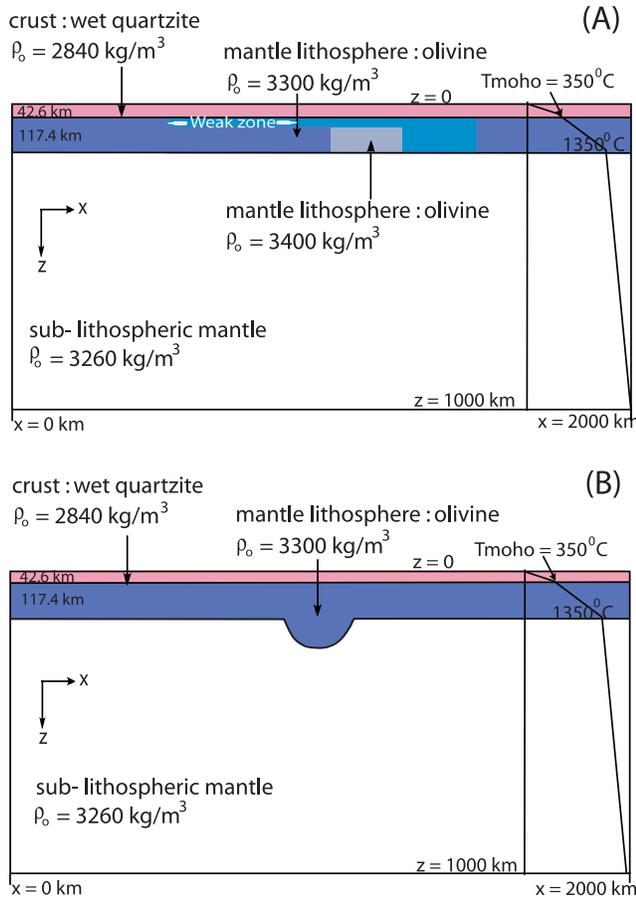
Figure 2. Illustration of the model geometry and setup for (A) mantle lithosphere delamination and (B) RT-type mantle instability experiments. A viscous flow law of $\dot{\varepsilon} = A\sigma^n \exp\left(\dfrac{-Q}{RT}\right)$ is used for mantle material (mantle lithosphere and sub-lithospheric mantle) where $\dot{\varepsilon}$ is the strain rate, T is temperature, and σ is differential stress. Variables A, n, Q, and R are the viscosity parameter, power exponent, activation energy, and ideal gas constant, respectively. On the basis of a strain rate of 10^{-15} 1/s and temperature of 1350°C, the viscous flow law results in an effective viscosity of the sub-lithospheric mantle of 10^{20} Pa s. For continental crust A = 1.1×10^{-28} Pa^{-4}/s, n = 4, and Q = 223 kJ/mol are used, based on wet quartzite [*Gleason and Tullis*, 1995]. For the crust an internal angle of friction $\phi = 15^0$ is used for a Coulomb yield criterion. A = 4.89×10^{-17} Pa$^{-3.5}$/s, n = 3.5, and Q = 535 kJ/mol are used for mantle material (mantle lithosphere and sub-lithospheric mantle) based on dry olivine [*Hirth and Kohlstedt*, 1996].

helping to interpret the deep lithospheric dynamics from surface geology.

2. Experimental Results
2.1. Model Description

[10] For our experiments, we used SOPALE, a plane strain, incompressible numerical code to study the thermo-mechanical behavior of the coupled crust and mantle.

SOPALE is based on the arbitrary Lagrangian-Eulerian finite element technique and as such is useful for treating finite deformations, and for tracking boundaries (surface topography) and internal particles (P-T paths) [*Fullsack*, 1995; *Pysklywec et al.*, 2002].

[11] Figures 2A and 2B shows the initial configuration of our experiments. In the models, the 160 km thick lithosphere is made up of 42.6 km thick buoyant crust ($\rho_0 = 2840$ kg/m^3, pink) and 117.4 km thick dense mantle lithosphere ($\rho_0 = 3300$ kg/m^3, dark blue) overlying an upper mantle region ($\rho_0 = 3260$ kg/m^3, gray). Density is also a function of temperature: $\rho(T) = \rho_0(1 - \alpha(T - T_0))$, where $\alpha = 2 \times 10^{-5}$ 1/K is the coefficient of thermal expansion and $T_0 = 25$°C is the reference temperature [*Tackley et al.*, 1994]. The assumed density variations are responsible for all motions in the box (gravitational acceleration g = 9.8 m/s^2); there are no imposed (internal or boundary) velocities in the models. The viscous response of the crust is based on a wet quartzite flow law [*Gleason and Tullis*, 1995] whereas the sub-crustal (mantle) material is governed by a dry olivine rheology [*Hirth and Kohlstedt*, 1996]. The crustal layer also yields according to a Coulomb failure law (Figure 2), so that the upper crust behaves in a brittle manner.

[12] The numerical (width) × (depth) resolution is 201 × 101 Eularian nodes and 601 × 301 Lagrangian nodes. Half of the Eularian and Lagrangian elements are concentrated in the top 160 km in order to enhance resolution in the lithosphere.

[13] The initial temperature profile is the same in both experiments (Figure 2). Thermal properties (thermal conductivity k = 2.25 W/m/K, heat capacity c_p = 1250 J/kg/K) are the same for all materials and we ignore radioactive heat production and shear heating in the model. The top boundary of the box is held at 25°C and the bottom boundary is held at 1523°C; heat flux across the side boundaries is zero. The 350°C Moho is based on estimates for the southern Sierra Nevada of California [*Lachenbruch and Sass*, 1977], as a region where both dripping and delamination have been postulated.

[14] The model has a free top surface, allowing topography to develop as the model evolves. The mechanical boundary conditions at the other three sides are defined by zero tangential stress and normal velocity ("free slip"). We have extended the depth of the solution space into the lower mantle so that the sinking mantle lithosphere material moves away from the lithosphere. Although the depth of the box is 1000 km, the effects of the endothermic olivine phase (γ-spinel structure to perovskite) change at 660 km depth [e.g., *Christensen and Yuen*, 1984] are not implemented because we wanted to allow downgoing mantle lithosphere to move away from the surface to the deeper levels of the mantle.

[15] Each of the experiments has several modifications to initiate either delamination or viscous dripping. In order to start the delamination, we inserted a low-viscosity weak zone, with a viscosity of 5×10^{19} Pa s, between a section of the crust and mantle lithosphere (Figure 2A). A series of numerical experiments indicated that this viscosity is sufficiently low to decouple the crust from mantle lithosphere, whereas an increase to 5×10^{20} Pa s appreciably retards the development of the delamination process.

[16] The inclusion of a low-viscosity weak zone to initiate delamination is an approach followed by other studies of the process [*Morency and Doin*, 2004; *Le Pourhiet et al.*, 2006]. The density of the mantle lithosphere over a 180 km wide, 80 km thick zone was increased to $\rho_o = 3400$ kg/m^3 in order to further facilitate the delamination. *Jull and Kelemen* [2001] and *Elkins-Tanton* [2005] suggest that the lower lithosphere can become significantly denser and gravitationally unstable because of transformations such as from granulite to eclogite. According to *Jull and Kelemen* [2001], the density of the lower crust may become 50–250 kg/m^3 denser at minimum pressures of less than 1.5 GPa and eventually the anomalously denser lower crust may descend/sink as a "blob" depending on the nature of the instability.

[17] For the viscous dripping models we introduce a perturbation to the base of the dense mantle lithosphere to initiate the descent. It has been suggested that such perturbations may arise as a result of lithospheric contraction and thickening [*Houseman and Molnar*, 1997] or eclogitic metamorphism of lower crust [*Kay and Kay*, 1993; *Ducea and Saleeby*, 1998; *Jull and Kelemen*, 2001].

[18] We emphasize that the intent of this work is not to consider the conditions that control the initiation and development of the dripping or delamination of the mantle lithosphere; this has been studied elsewhere [*Conrad and Molnar*, 1997; *Jull and Kelemen*, 2001; *Morency and Doin*, 2004]. Rather, we set up conditions that will start these removal events and focus on various facets of the resulting near-surface dynamics.

[19] We present our results in dimensionless time. This is motivated by variations in effective viscosity between the three models that give rise to variations in the dimensional times of events in the models. As a characteristic timescale, we chose the time that it takes the descending mantle lithosphere to traverse the upper mantle and reach the bottom of the solution space. (The characteristic timescales for DEL, DRIP-1, and DRIP-2 are 4.5 Myrs, 21 Myrs, and 5.7 Myrs, respectively.) The non-dimensional times based on (variable) material deformation are more comparable and less influenced by variations in viscosity between models.

[20] The scaling of time by a deformational process (descent) is particularly suitable for the early and intermediate stages of the model evolution. The removal of mantle lithosphere is sufficiently rapid in all the models that thermal diffusion is not a significant factor during descent. It may be more appropriate, though, to scale time based on thermal diffusion during a longer timescale ($\sim t > 5$) when removal of mantle lithosphere is largely finished and thermal relaxation becomes dominant [e.g., *Conrad*, 2000]. However, the cooling and re-establishment of lithosphere occurs on similar timescales for all of our models and for this contribution the late-stage evolution is of secondary importance to the dynamics during removal.

2.2. Dripping and Delaminating Mantle Lithosphere

[21] Figure 3A shows the evolution of a delamination model. By t = 0.26 the mantle lithosphere is peeling away from the crust. As the lithosphere delaminates, the lower-viscosity sub-lithospheric mantle flows into the area vacated by mantle lithosphere. This results in appreciable advection of mantle heat upward (Figure 3A, inset). The hot sub-lithospheric isotherms are deflected toward the crust as the material progressively intrudes into the mantle lithosphere gap. The delamination progresses rapidly and by t = 0.84 a $\sim$800 km wide section of mantle lithosphere has been removed, exposing the crust to sub-lithospheric mantle. The width of the breach is dependent on the width of the weak decoupling layer. Rather than peeling away as a single slice, the delaminated fragment of mantle lithosphere eventually detaches into separate fragments as it falls into the mantle. The sub-lithospheric mantle flow becomes more subdued as the delamination comes to an end and over the longer course of the experiment the material in the mantle lithosphere gap cools down to produce new lithosphere.

[22] To compare to the delamination model, two different RT-instability models are shown: DRIP-1 and DRIP-2. They are physically and geometrically similar models, except that DRIP 2 has temperature-independent behavior for mantle lithosphere, whereas DRIP-1 has temperature-dependent mantle lithosphere viscosity. Both models use non-Newtonian (n = 3.5) viscosities. In comparison to Newtonian (n = 1) fluids, the non-linear rheology will tend to localize deformation since viscosity is reduced as strain rates increase. This tends to limit the amount of material that is involved in the mantle lithosphere drip [*Houseman and Molnar*, 1997]. In terms of controlling parameters, For the DRIP-1, we use the flow law and controlling parameters described in Figure 2, whereas the DRIP-2 uses on both sides the same flow law but with parameters Q = 0 and A = 10^{-38} Pa^{-n}/s. On the basis of strain rates of 10^{-13} 1/s to 10^{-17} 1/s that are characteristic of flow in the models, this results in a mantle lithosphere viscosity ranging from 2.5 $\times$ 10^{20} Pa s to 1 $\times$ 10^{23} Pa s.

[23] In both models, the lithospheric perturbation induces a drip-style downwelling of the mantle lithosphere (Figures 3B and 3C). However, in the temperature-dependent experiment (Figure 3B) only the lowermost portion of the mantle lithosphere is dripping, as the warmer/weaker region of the lithosphere. Also, this deformation is spread over a rather broad lateral extent. In the temperature-independent case (Figure 3C), most of the mantle lithosphere layer is being deformed, but over a localized lateral extent. Clearly, DRIP-2 is descending more quickly than DRIP-1 since there is greater mass of unstable mantle lithosphere with DRIP-2 than DRIP-1. The amount of material participating in the instability has been explained as an "available buoyancy" that controls the growth rate of the drip [*Conrad and Molnar*, 1999].

2.3. Surface Topography

[24] As the mantle lithosphere starts to delaminate (t = 0.13), it causes subsidence of the crust with an amplitude of approximately −1100 m (Figure 4A). This subsidence is a result of the loading on the surface of the peeling/descending mantle lithosphere. Adjacent topography highs at x = $\sim$1300 km and x = $\sim$800 km arise from surrounding upwelling return flow of sub-lithospheric mantle.

[25] By t = 0.26, the negative surface deflection reaching a maximum amplitude of 3.5 km. A significant length of delaminating slab is pulling down on the crust at the location where the mantle lithosphere is still attached to the surface (Figure 3A). Enhanced uplift occurs on the right side of the depression as hot mantle material is flowing into
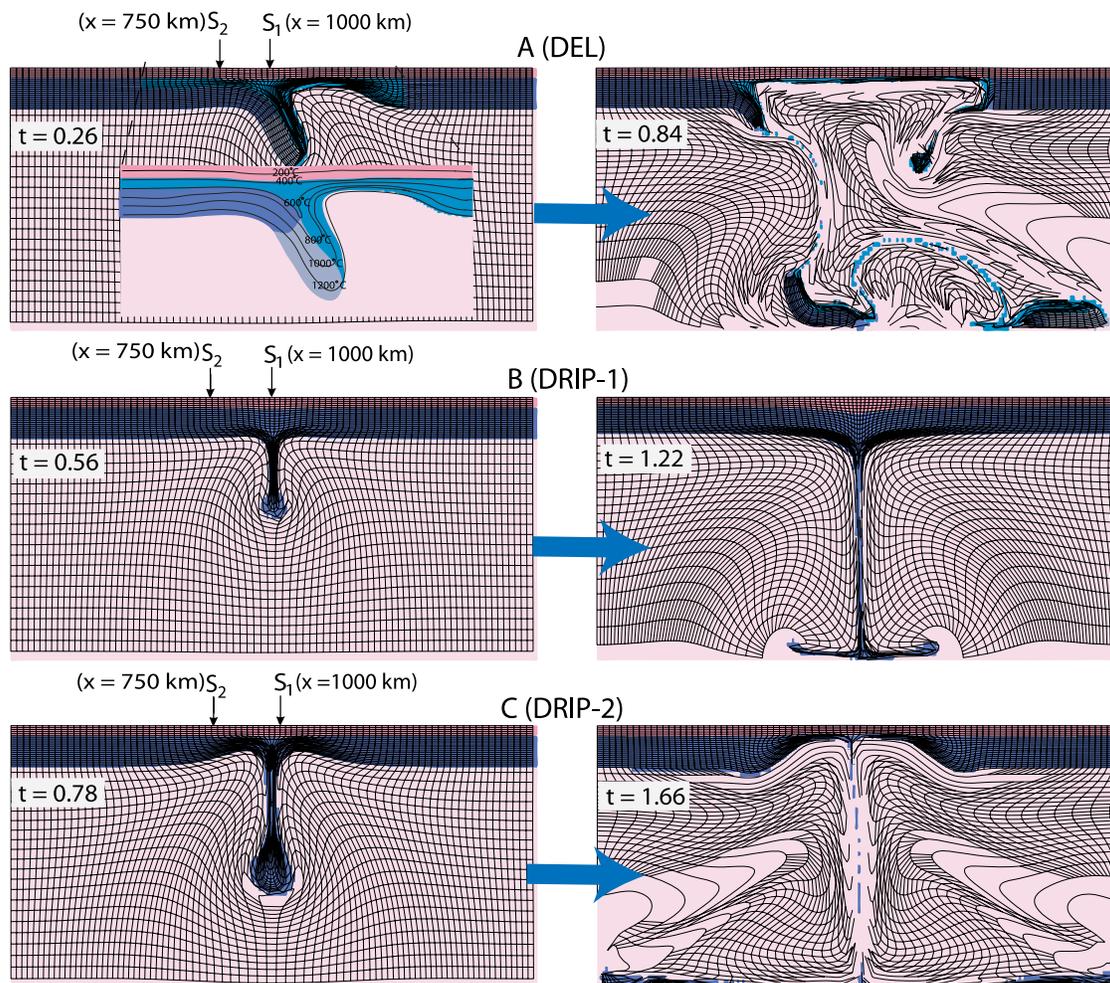
Figure 3. Evolution of the models: (A) DEL delamination, (B) DRIP-1 viscous dripping with non-linear temperature-dependent rheology, and (C) DRIP-2 viscous dripping with non-linear, temperature-independent rheology. Each frame shows material colors (see Figure 2) and deformed Lagrangian mesh. The latter is plotted at one-half actual resolution; mesh is initially even rectangular. Inset in Figure 3B shows isotherms of zoomed region. S_1 and S_2 indicate locations of sections for P-T-t analyses. Extremely deformed Lagrangian elements are not plotted in the figures. Although there is high distortion of this mesh, it does not affect the numerical accuracy of the models since computations are performed on the relatively undistorted Eulerian mesh in the arbitrary Lagrangian-Eulerian finite element technique.

the lithosphere breach vacated by the delaminating lithosphere both sides of this negative topography, again due to return mantle flow. The signal of topography is becoming more asymmetrical as the delamination progresses in these very early stages. The amplitude of the negative deflection is very high; we ascribe this to the extra forcing by the anomalously high-density lithospheric block that was used to initiate delamination.

[26] By $t = 1.26$ most of the mantle lithosphere has been removed and the surface topography is characterized by a broad uplift ($t = 1.26$; Figure 4A). Now, most of this uplift is associated with the replacement of the lithospheric mantle by buoyant sub-lithospheric mantle, as there is relatively little mantle flow across the vacated lithospheric zone. The exception to this is at $x = 400$ km where there is still some active delamination that induces enhanced local subsidence/uplift. It is important to note that through the delamination process the locus of the main topography anomaly migrates

to the left. That is, the topography is spatially transient, as it responds to the peeling lithosphere.

[27] In the DRIP-1 experiment a negative topography initially develops above the descending RT instability reaching a maximum depression of 600 m ($t = 0.30$; Figure 4B). This symmetric topography is supported by the actively descending/dripping mantle lithosphere (Figure 3B). Eventually, the subsidence inverts to uplift ($t = 0.60 - 0.90$). This is a result of the decrease in the downwelling forces as the descending mantle lithosphere is necking and narrowing, and reaches the bottom of the box. The topography is now dominated by isostatic uplift associated with the flow-induced crustal contraction and thickening [e.g., *Pysklywec and Shahnas*, 2003; *Pysklywec and Cruden*, 2004]. The physical development and the progression of these events of DRIP-2 is similar with DRIP-1: There is initial surface subsidence, followed by uplift as a result of the interplay between the dynamic effects of the mantle flow and crustal
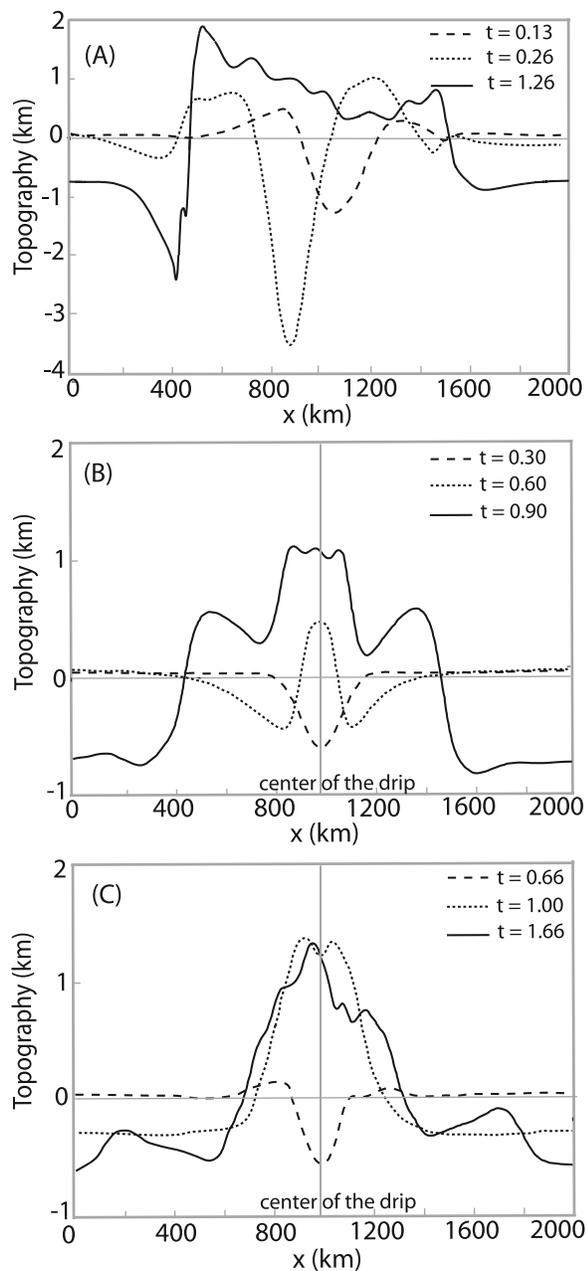
Figure 4. Plots of surface topography at three time intervals for models: (A) delamination, (B) DRIP-1, and (C) DRIP-2.

thickening. However, with DRIP-2, the more localized removal of mantle lithosphere material is responsible for a more focused band of crustal contraction/thickening and isostatic compensation by the asthenospheric mantle.

[28] As in the delamination model, both drip experiments show an initial phase of subsidence, followed by uplift. However, the drip models show clearly symmetrical topography signals that remain fixed in location above the downwelling mantle lithosphere. This assumes the mantle lithosphere instability does not migrate with respect to the overlying plate.

2.4. Moho Temperatures

[29] The Moho temperatures were tracked in all experiments to consider the thermal expression of the crust to the mantle lithosphere removal style. In the numerical model, we used two different methods to illustrate the varying Moho temperatures. Firstly, a time series plot of zonal average and maximum Moho temperatures for each of the experiments was tracked (Figures 5–7A). This is done by calculating maximum and average temperatures at a depth between 38.4 and 41.6 km and width between 500 km and 1500 km. The time series demonstrates how temperature changes in a Moho "zone" in a Eulerian reference frame. The lateral limits (x = 500 and 1500 km) to the Moho zone were chosen to focus on the location of delamination and drip at the center of the computational box. Secondly, we plotted the temperature of specific numerical particles along the entire base of the crust (x = 0–2000 km) at discrete time periods (Figures 5 and 7B). The particles started at the initial Moho depth of 42.6 km, notably couple of kilometers deeper than Eulerian depths, and subsequently track the evolving temperature of these particles in a Lagrangian framework.

[30] Until t = 1.00, there is a rapid increase of the maximum Moho temperatures reaching more than 600°C (Figure 5A). This is a consequence of the upwelling of the asthenospheric material into the lithospheric gap. Subsequently, there is more gradual increase of the maximum and average temperature in this zone as more of the lithosphere delaminates away and the hot mantle temperatures conduct heat into the crust. It reaches a maximum of ∼1200°C by about t = 5.00. In Figure 5B the temperatures of the "Moho particles" are plotted at three discrete intervals: t = 0.26, t = 0.64 and t = 1.00 At t = 0.26, the base of the crust is heated to ∼400°C. As most mantle lithosphere is removed and a broader zone of Moho is heated by t = 0.64, a wider swath of these particles has increased temperature up to ∼500°C in average. By t = 1.00, after the main delamination event, the full range of particles above the lithospheric gap experience elevated temperatures.

[31] Calculated Moho temperatures for DRIP-1 and DRIP-2 show significant differences. While the maximum Moho temperature values for DRIP-1 show very slight changes (Figure 6A), temperatures obtained from DRIP-2 are close to that of the delamination model (Figure 7A). For DRIP-1, the maximum temperatures at the base of the crust do not even reach 400°C and the average temperature of the Moho actually decreases slightly. There is only subtle warming of the Moho particles over time as they are pulled/pushed to greater depths (see below). Clearly, the crust is quite insulated from the thermal effects associated with the DRIP-1 downwelling, which occurs mostly in the lower portion of the mantle lithosphere (Figure 3B).

[32] The initial stages of the Moho temperatures of the DRIP-2 are similar with DRIP-1: As the mantle lithosphere instability grows until ∼t = 1.25 the crust experiences relatively little thermal perturbation (Figure 7A). During this phase, the advection of temperatures downward with descending mantle lithosphere helps to keep the Moho region relatively cool (Figure 7C). Eventually, the dripping mantle lithosphere detaches and hot sub-lithospheric mantle material flows into the void, resulting in a rapid increase in lower-crust zonal temperatures (Figure 7A). By t = 2.19,
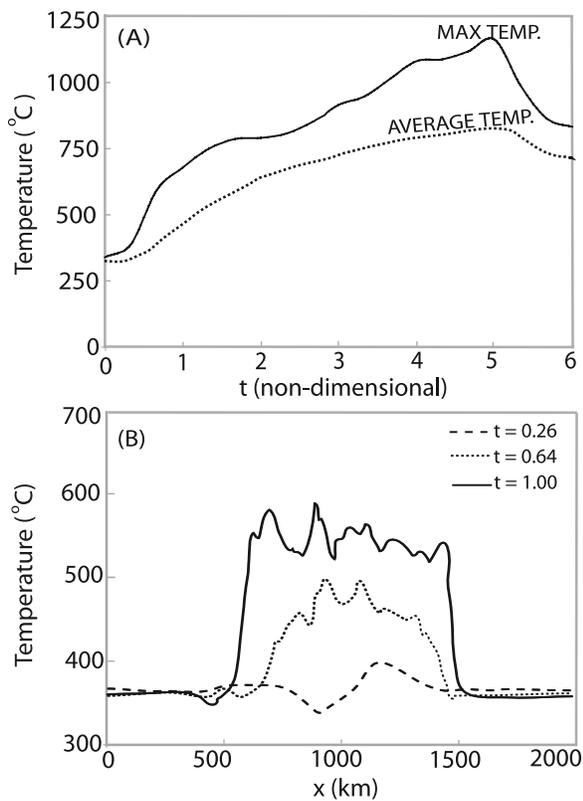
Figure 5. For the delamination model. (A) Plots of zonal maximum and average temperatures at 42.6-km depth as a function of time (see text for explanation). (B) Particle temperature of "Moho particles" at t = 0.26, t = 0.64, and t = 1.00.

discrete particles in the lower crust show heating to about 600°C across a ∼1000 km wide band corresponding to the removal area (Figure 7B). Clearly, the rheology of the mantle lithosphere, which governs the portion of mantle lithosphere that is removed (i.e., DRIP-1 versus DRIP-2), has a first-order effect on the thermal expression of dripping lithosphere in the crust. With almost complete removal the thermal signature is similar to that of delamination.

[33] The high temperatures decrease quite rapidly from their peak at ∼t = 2.5 (Figure 7A). We ascribe this to continual flow of surrounding mantle lithosphere into the lithospheric gap which causes cooling in this zone. The delamination model does not experience this rapid drop in temperature as the stronger (more plate-like) mantle lithosphere does not have the same predilection for lateral flow.

2.5. P-T Histories

[34] We constructed pressure-temperature-time paths (P-T-t) by tracking individual groups of Lagrangian particles within the deforming crustal material domain. We focused on two vertical profiles locations: At S_1 (x = 1000 km) and S_2 (x = 750 km) which correspond to the middle of the box and an intermediate distance across the removal zone (Figure 3). For these two locations, we track the pressure and temperature at positions in the upper (z = 7 km), middle (z = 19 km), and lower (z = 39 km) crust. The pressure tracked is actually the lithostatic pressure associated with the burial or uplift of material. That is, it is derived as pressure $p = \rho * g * h$, where h is the thickness of the

overburden material above the point, g is gravitational acceleration, and ρ is the density of the overburden material. The additional "dynamic" pressure is negligible compared to the lithostatic pressures for these types of non-convergent plate models. Surface erosion is not implemented in the models.

[35] Figure 8A shows the P-T-t path of the mantle lithosphere delamination (DEL) model. S_1 (x = 1000 km) of 39 km depth reaches its maximum burial depths rapidly at t = 0.38 with a maximum pressure of ∼11 kbar. This corresponds to modest extra burial of approximately three kilometers as that portion of lower crust is pulled down by the delaminating mantle lithosphere. Subsequently, the P-T history is dominated by heating of ∼350°C until t = 2.8. This is accompanied by decompression of 2.3 kbar, or about 9 km of tectonic exhumation. The P-T-t trends of the shallower particles at z = 16 km and z = 7 km depths for same section (S_1) are similar in that they are characterized by decompression heating. However, the temperature increases are slower and smaller at these depths, as the mantle heat has to conduct through the crust.

[36] The progression of the P-T change is essentially mirrored in the lithospheric section at S_2 (x = 750 km), except that the events are delayed by several million years as the mantle lithosphere delaminates in that direction. For example, the maximum burial of the deep crust point to 12 km is reached at t = 0.6 and maximum heating is reached at t = 4.2. This suggests that the metamorphic signal in the
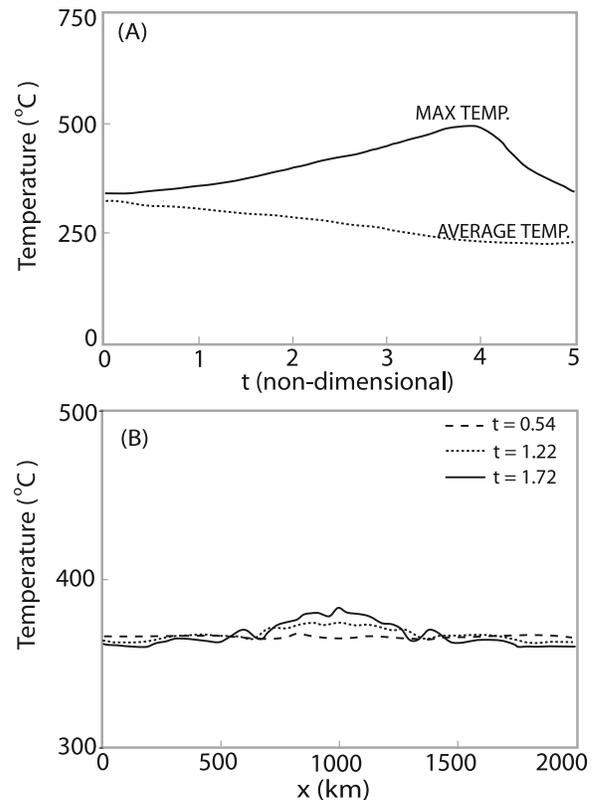

Figure 6. For the DRIP-1 model. (A) Plots of zonal maximum and average temperatures at 42.6-km depth as a function of time (see text for explanation). (B) Particle temperature of "Moho particles" at t = 0.54, t = 1.22, and t = 1.72.
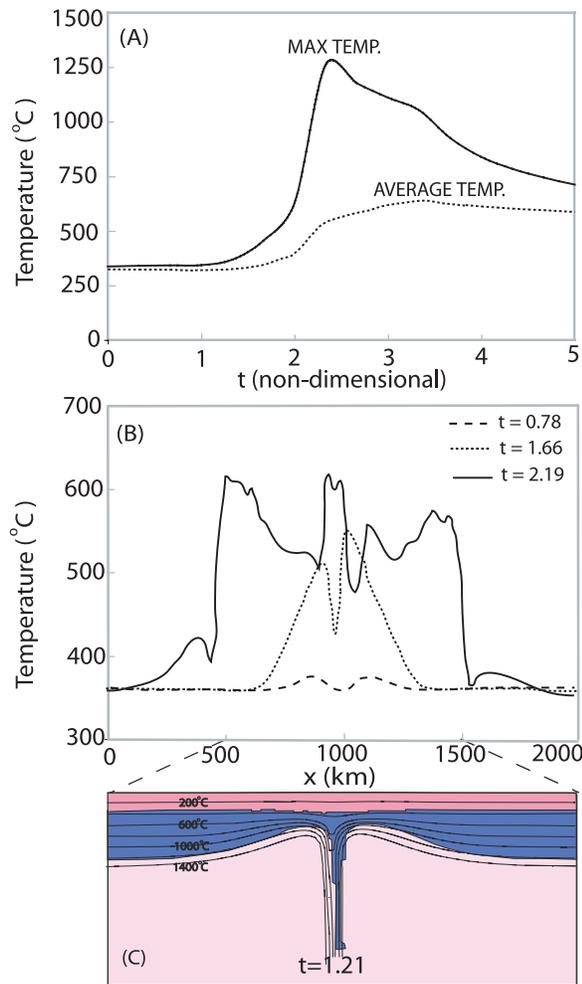
Figure 7. For the DRIP-2 model. (A) Plots of zonal maximum and average temperatures at 42.6-km depth as a function of time (see text for explanation). (B) Particle temperature of "Moho particles" at t = 0.78, t = 1.66, and t = 2.19.

The shallower points, again, demonstrate a similar behavior, but with more modest pressure increases.

[38] Interestingly, the P-T-t paths associated with experiment DRIP-2 show patterns more akin to the delamination model. Lower crust at S_1 increases to a pressure of 12.1 kbar at t = 1.1 (Figure 8C), corresponding to the time of vigorous mantle lithosphere dripping (Figure 3C). After this time, there is a pressure decrease to 8 kbar and heating to 600°C until t = 3.3. At section S_2 the P-T-t path is different: It does not experience the initial burial and most heating occurs prior to the modest final uplift. This occurs also in the shallower crustal points.
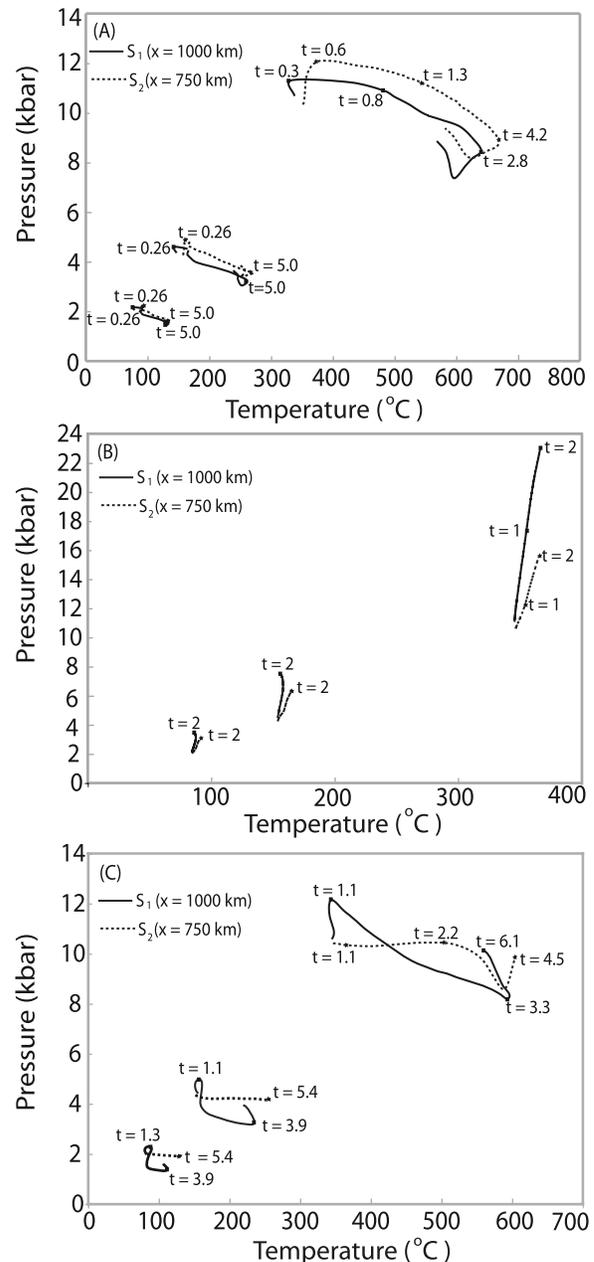
crust of delamination would be increased in temperatures and modest decompression between t = 0.6 and t = 4.2; essentially clockwise P-T paths dominated by temperature increase. This metamorphic signal would migrate as a type of "a single metamorphic wave" with the delaminating mantle lithosphere.

[37] The P-T evolution of DRIP-1 is very different. It is dominated by slow pressure increase and very modest changes in temperature (Figure 8B). For example, the lower crust at section S_1 shows an increase in pressure of ~12 kbar over t = 2.0, which represents a burial of 86 km. This is clearly a portion of the crust that is being entrained downward within the mantle lithosphere drip [e.g., *Pysklywec and Cruden*, 2004]. The package is relatively better thermally insulated as it warms only ~50°C over this time. In comparison, at section S_2 the lower crust is buried to a depth of only 59 km. The effects of crustal thickening and burial are most extreme directly above the mantle lithosphere downwelling. Indeed at distances sufficiently far from the drip, the crust can undergo extension and uplift during these stages instead [*Pysklywec and Cruden*, 2004].

Figure 8. Pressure-temperature paths for particles in the upper (z = 7 km), middle (z = 19 km) and lower (z = 39 km) crust at sections S_1 (x = 1000 km) and S_2 (x = 750 km). Paths for model: (A) delamination, (B) DRIP-1, and (C) DRIP-2.
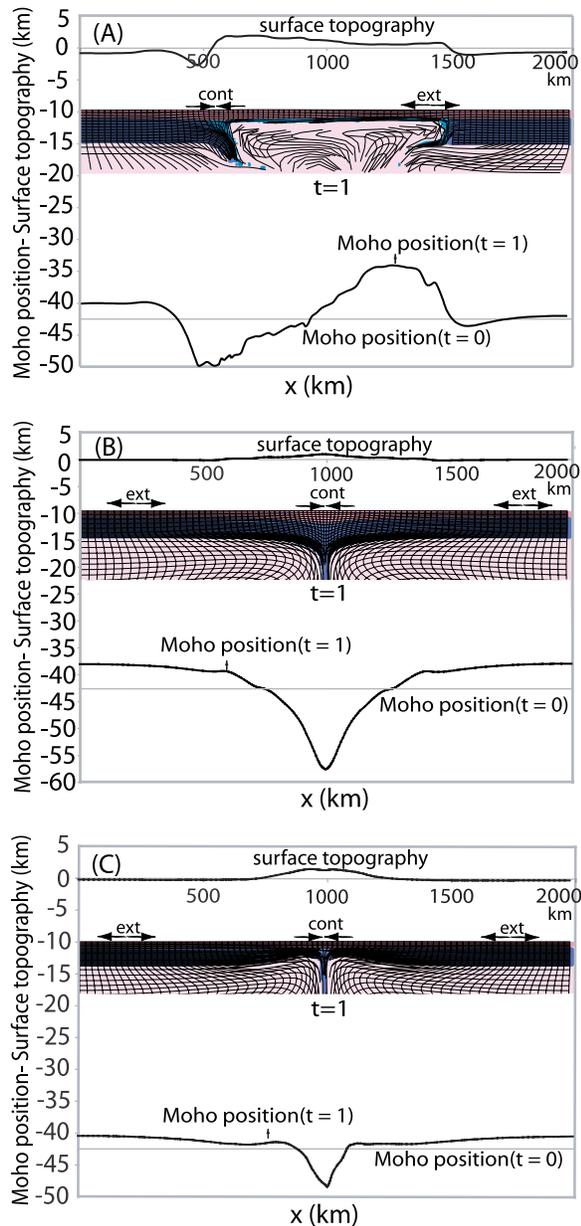
Figure 9. Plots of Moho position and surface topography across a portion of each model at t = 1.0: (A) delamination, (B) DRIP-1, and (C) DRIP-2. Included for each is a frame displaying material colors and Lagrangian mesh (plotted at one-half actual resolution). "Ext" refers to extension.

[39] The variation in behavior between sections differentiates the metamorphic signature of crustal material between the delamination model and DRIP-2. The delamination P-T-t paths at the different sections were essentially the same, but with a temporal shift associated with the peeling lithosphere. For DRIP-2, the sections show varying behavior depending on their lateral position since the mantle lithosphere drip is not moving laterally with respect to the surface crust.

2.6. Crustal Deformation

[40] Lastly, we investigate styles of finite crustal deformation and structure that may be characteristic of the mantle lithosphere removal mechanisms. Differences are highlighted by: (1) plotting the variation of the Moho position and surface topography to illustrate variations in crustal thickness and (2) displaying the Lagrangian cells in the lithosphere, which are initially even rectangular, and so show accumulated deformation in their contorted state.

[41] For the delamination experiment at t = 1.0, the deformed Lagrangian cells demonstrate that above the delaminating lithosphere (at x = ~500 km) there is contraction (Figure 9A). The downgoing plate is pulling crustal material into the zone above the delaminating hinge. This correlates with thickened crust as the Moho is deflected downward by approximately 7.5 km. It is worthwhile to note that the surface topography is negative in this region despite the thickened crust. Apparently, the sub-crustal loading of the delaminating mantle lithosphere is overwhelming isostatic (uplift) effects associated with thickening crust. On the other side of the lithospheric gap (at x = ~1250 km), there is extension of the crustal elements. The crust here has been thinned by up to 7.5 km. We attribute the extension/thinning to several factors. Firstly, the sub-lithospheric mantle flow into the gap and laterally may be helping pull apart the crust. Secondly, previously contracted/thickened crust may be in gravitational collapse as the delaminating mantle has moved away. Note again, that although the crust is thin, the surface topography is not anomalously low. This suggests that surface topography is dynamically supported by underlying mantle flow.

[42] Figure 9B shows the variation in the crustal thickness and surface topography at t = 1.0 for DRIP-1. At this stage, it is observed that dripping mantle lithosphere causes lateral crustal flow toward the center, which results in contraction and crustal thickening, while the distal regions experience broad bilateral or symmetrical type extension with contraction/thickening. The deflection of the Moho directly above the drip is consistent with interpretations of crustal structure for the southern Sierra Nevada from receiver function studies [*Zandt et al.*, 2004]. This work suggests that the Moho is characterized by a "V"-shaped profile by the entrainment of the viscous crust into the mantle lithosphere, much like that shown in Figure 9B.

[43] DRIP-2 at t = 1.0 shows a confined zone of contractional deformation, with shortened Lagrangian cells within ~100 km of each side of the center of the downgoing mantle lithosphere (at x = 1000 km; Figure 9C). Just outside this zone, on both flanks, the crust has been extended. This contraction is accompanied by a thin region of crustal thickening as crust is entrained downward into the mantle lithosphere drip. The localized thickening occurs within a broader (~800 km) zone of thinned crust. The crustal extension and thinning may be due to collapse of previously developed topography (e.g., Figure 4C) and small-scale mantle flow in the mantle lithosphere gap as material is pulled from the flanks toward the center of the downwelling. The symmetric and highly localized nature of deformation of the crust in DRIP-2 clearly distinguish it from both the delamination and alternate drip model.

3. Conclusions and Discussion

[44] In conclusion, there are similarities in the surface crustal response to dripping or delaminating mantle litho-

sphere, but the models demonstrate that there may be several surface (or near-surface) diagnostic expressions of delaminating or dripping mantle lithosphere. The numerical experiments demonstrate the following:

[45] 1. Surface topography for both drip models shows initial subsidence with a subsequent phase of uplift, the locus of which stays fixed above the downwelling. Geometrically, the surface topography associated with both drip events is symmetric. In the delamination model, there is paired subsidence and uplift that migrates as the mantle lithosphere peels away from the crust. The surface topographic expression is distinctly asymmetric.

[46] 2. The thermal expression of delamination is characterized by a rapid increase in Moho temperature soon after the lithosphere begins to peel away. The thermal spike (up to near mantle temperature) migrates along the lithospheric gap, and the crustal temperature in this zone continues to increase while sub-lithospheric flow is active. Depending on the style of dripping (i.e., how much mantle lithosphere is removed), there can be appreciable thermal perturbation of the crust (DRIP-2), or very little (DRIP-1). Delamination seems to be more efficient as a crustal heating mechanism since the mantle lithosphere gap is maintained for a longer time because of the inherent characteristics of the process. That is, with viscous dripping, surrounding cool mantle lithosphere will flow into the lithospheric gap, causing a more rapid decrease of the elevated crustal temperatures. The thermal perturbations associated with dripping mantle lithosphere are centered and fixed above the downwelling, whereas with delamination the locus of peak temperature migrates as the peeling lithosphere does.

[47] 3. The P-T evolution of the crust above delaminating mantle lithosphere shows a clockwise path dominated by temperature increase and a modest initial pressure increase and gradual decompression. This P-T signature migrates across the crust as the mantle lithosphere delaminates, almost as a type of "single metamorphic wave". With partial dripping of the mantle lithosphere (DRIP-1), the overlying crust will show very little thermal variation, but pressure increases associated with burial/thickening can occur. With wholesale dripping of the mantle lithosphere, the crust directly above the drip may experience (slower) temperature increase and some pressure increase then decrease as in the delamination model. However, unlike with delamination, where P-T path is essentially repeated (migrated) from one location to another, e.g., from points S_1 (x = 1000 km) to S_2, (x = 750 km). The crust at the periphery of the drip will experience a different P-T evolution at S_1 (x = 1000 km) and S_2 (x = 750 km) such as, varying burial and exhumation degrees.

[48] 4. Mantle lithosphere delamination induces a zone of contraction and crustal thickening just above the hinge of the peeling mantle lithosphere. A region of extension occurs at the distal end of the lithospheric gap as sub-lithospheric mantle flows up and laterally to replace delaminating lithosphere. The contraction zone sweeps across the crust as the mantle lithosphere peels away. The drip models also drive contraction and crustal thickening centered on the downgoing mantle lithosphere. However, in these models there is symmetric crustal extension on both sides. Depending on mantle lithosphere rheology, the deformation may be very localized to the central axis of the downwelling

(DRIP-2) or broadly distributed about it (DRIP-1). Deep entrainment of crust into the descending mantle lithosphere represents an extreme mode of crustal thickening.

[49] It is important to emphasize that our derived P-T-t paths represent the pressure-temperature history of the crustal packages to only the delamination/drip event. There may be pre-/syn-/post-tectonic events in addition to the mantle lithosphere removal event that modifies the P-T-t path. For example, with simultaneous plate convergence, burial and enhanced pressure increase could occur. The results demonstrate that the crust, follows a similar P-T pattern at three (upper, mid, and lower) levels, but with different amplitudes. Not surprisingly, though, the most apparent signature is in the lower crust. *Platt et al.* [1998] have used P-T paths from rocks extracted from the Alboran seafloor and in the Betics, beneath which mantle lithosphere removal is proposed. The authors suggest that mantle drip/convective removal is more plausible to the region, since P-T paths indicate the exhumation in the metamorphic rocks for last 30 Myrs due to the crustal extension that is responsible for the exhumation of these rocks.

[50] Here we show one delamination and two of the drip models from a range of numerical experiments that were run. On the basis of the convention of delamination that we are considering, namely that the whole mantle lithosphere must be removed as a coherent slice, the type of model is fairly tightly confined. Models with alternate rheologies and densities (but still delaminating) modified the amplitude and timing of the surface response, but not the general character. On the other hand, the drip models had an unconstrained aspect that was particularly important for altering the effect on the crust: the amount of mantle lithosphere that was viscously removed. We chose DRIP-1 and DRIP-2 as representative models of partial removal and full removal, respectively. Indeed, the results show that care must be taken in interpreting large-scale lithospheric dynamics from surface observables as one geodynamic mechanism can affect the crust in different ways depending on a specific aspect of the removal event. Again, we emphasize that the purpose of this work was not to examine the parameters controlling the removal mechanisms. Rather, we have identified and shown these three experiments as representative models of the fundamental modes of removal and surface response.

[51] One of the assumptions we have made in the models is that the dripping mantle lithosphere does not migrate laterally with respect to the overlying crust. We recognize that it is possible that a viscous mantle lithosphere instability could migrate, possibly within the presence of a larger background mantle flow field or as a result of other unbalances. This migration may arise as a result of lateral variations in lithospheric (mantle or crust) rheology or thickness. *Houseman et al.* [2000] suggest that the nature and the proximity of the drip to the convergence zone may change, depending on the rate of the convergence from a multiple sheets like to single downwelling. Three-dimensional physical scaled analogue models of dripping mantle lithosphere showed, for example, lateral movement of the instability, probably as a consequence of interaction with adjacent unstable mantle lithosphere [*Pysklywec and Cruden*, 2004]. The attendant surface deformation followed this drip migration. The surface topography in these three-

dimensional models took on a generally radial geometry to reflect the cylindrical (rather than sheet-like) mantle lithosphere downwelling. Distal zones of extension were separated by radial spoke-like bands of downwelling and crustal contraction [*Pysklywec and Cruden*, 2004]. It has been suggested that a drip structure beneath the southern Sierra Nevada has shifted over the last 4–5 Myrs [*Zandt*, 2003]. They interpret this from a migrating locus of surface volcanism that they attribute to return flow of hot mantle associated with the downgoing mantle lithosphere. We note that our results suggest that such an observation may be more consistent with delaminating mantle lithosphere and a further investigation taking into account all the factors described above (in conjunction with other geophysical evidence) may help differentiate the mechanism. Nevertheless, lateral motion of the drip would alter some of the conclusions we make, above, and should be taken into account when interpreting the results.

References

Beck, S. L., and G. Zandt (2002), The nature of orogenic crust in the central Andes, *J. Geophys. Res.*, *107*(B10), 2230, doi:10.1029/2000JB000124.

Bird, P. (1978), Initiation of intracontinental subduction in the Himalayas, *J. Geophys. Res.*, *83*, 4975–4987.

Bird, P. (1979), Continental delamination and the Colorado Plateau, *J. Geophys. Res.*, *84*, 7561–7571.

Buck, W. R., and M. N. Toksoz (1983), Thermal effects of continental collisions: Thickening a variable viscosity lithosphere, *Tectonophysics*, *100*, 53–69.

Conrad, C. P., and P. Molnar (1997), The growth of Rayleigh-Taylor-type instabilities in the lithosphere for various rheological and density structures, *Geophys. J. Int.*, *129*, 95–112.

Conrad, C. P., and P. Molnar (1999), Convective instability of a boundary layer with temperature and strain-rate-dependent viscosity in terms of "available buoyancy", *Geophys. J. Int.*, *139*, 51–68.

Conrad, C. P. (2000), Convective instability of thickening mantle lithosphere, *Geophys. J. Int.*, *143*, 52–70.

Christensen, U. R., and D. A. Yuen (1984), The interaction of a subducting slab with a chemical or phase boundary, *J. Geophys. Res.*, *89*, 4389–4402.

Cloos, M., B. Sappie, A. Quarles van Ufford, R.J. Weiland, P. Q. Warren, and T. P. Mc Mahon (2005), Collisional delamination in New-Guinea: The geotectonics of subducting slab breakoff, *Geol. Soc. Am. Spec.*, *400*, 48 pp.

Ducea, M. N., and J. B. Saleeby (1998), A case for delamination of the deep batholithic crust beneath the Sierra Nevada, California, *Int. Geol. Rev.*, *40*, 78–93.

Elkins-Tanton, L. T. (2005), Continental magmatism caused by lithospheric delamination, in *Plates, Plumes and Paradigms*, edited by G. Foulger et al. *Geol. Soc. Am. Spec. pap.*, *388*, 449–461, doi: 10.1130/2005.2388(27).

England, P., and G. A. Houseman (1989), Extension during continental convergence, with application to the Tibetan Plateau, *J. Geophys. Res.*, *94*, 17,561–17,579.

Fullsack, P. (1995), An arbitrary Lagrangian-Eularian formulation for creeping flows and applications in tectonic models, *Geophys. J. Int.*, *120*, 1–23.

Gleason, G. C., and J. Tullis (1995), A flow law for dislocation creep of quartz aggregates determined with the molten salt cell, *Tectonophysics*, *247*, 1–23.

Hirth, G., and D. L. Kohlstedt (1996), Water in the oceanic upper mantle: Implications for rheology, melt extraction and the evolution of the lithosphere, *Earth Planet. Sci. Lett.*, *144*, 93–108.

Houseman, G. A., D. P. McKenzie, and P. Molnar (1981), Convective instability of a thickened boundary layer and its relevance for the thermal evolution of continental convergent belts, *J. Geophys. Res.*, *86*, 6115–6132.

Houseman, G. A., and P. Molnar (1997), Gravitational (Rayleigh-Taylor) instability of a layer with non-linear viscosity and convective thinning of continental lithosphere, *Geophys. J. Int.*, *128*, 125–150.

Houseman, G. A., E. A. Neil, and M. D. Kohler (2000), Lithospheric instability beneath the Transverse Ranges of California, *J. Geophys. Res.*, *105*, 16,237–16,250.

Jones, C. H., G. L. Farmer, and J. Unruh (2004), Tectonics of Pliocene removal of lithosphere of the Sierra Nevada, California, *Geol. Soc. Am. Bull.*, *116*, 1408–1422.

Jull, M., and P. B. Kelemen (2001), On the conditions for lower crustal convective instability, *J. Geophys. Res.*, *106*, 6423–6446.

Kay, R. W., and S. M. Kay (1993), Delamination and delamination magmatism, *Tectonophysics*, *219*, 177–189.

Keskin, M. (2003), Magma generation by slab steepening and break off beneath a subduction accretion complex: An alternative model for collision-related volcanism in Eastern Anatolia, Turkey, *Geophys. Res. Lett.*, *30*(24), 8046, doi:10.1029/2003GL018019.

Lachenbruch, A. H., and J. H. Sass (1977), Heat flow in the United states and the thermal regime of the crust, in *The Earth's Crust, Its Nature and Physical Properties*, *Geophys. Monogr. Ser.*, vol. 20, edited by J. G. Heacock, pp. 626–675, AGU, Washington, D. C.

Le Pourhiet, L., M. Gurnis, and J. B. Saleeby (2006), Mantle instability beneath the Sierra Nevada Mountains in California and Death Valley extension, *Earth Planet. Sci. Lett.*, *25*, 104–119.

Lenardic, A., and W. M. Kaula (1995), More thoughts on convergent crustal plateau formation and mantle dynamics with regard to Tibet, *J. Geophys. Res.*, *100*, 15,193–15,203.

Manley, C. R., A. F. Glazner, and G. L. Farmer (2000), Timing of volcanism in the Sierra Nevada of California: Evidence for Pliocene delamination of the batholithic root?, *Geology*, *28*, 811–814.

Molnar, P., G. A. Houseman, and C. P. Conrad (1998), Rayleigh-Taylor-type instability and convective thinning of mechanically thickened lithosphere: Effects of non-linear viscosity decreasing exponentially with depth and of horizontal shortening of the layer, *J. Geophys. Res.*, *133*, 568–584.

Morency, C., and M.-P. Doin (2004), Numerical simulations of mantle lithospheric delamination, *J. Geophys. Res.*, *109*, B03410, doi:10.1029/2003JB002414.

Neil, E. A., and G. A. Houseman (1999), Rayleigh-Taylor instability of the upper mantle and its role in intraplate orogeny, *Geophys. J. Int.*, *138*, 89–107.

Pysklywec, R. N., C. Beaumont, and P. Fullsack (2002), Lithospheric deformation during the early stages of continental collision: Numerical experiments and comparison with South Island, New Zealand, *J. Geophys. Res.*, *107*(B7), 2133, doi:10.1029/2001JB000252.

Pysklywec, R. N., and M. H. Shahnas (2003), Time-dependent surface topography in a coupled crust-mantle convection model, *Geophys. J. Int.*, *154*, 268–278.

Pysklywec, R. N., and A. R. Cruden (2004), Coupled-crust mantle dynamics and intraplate tectonics: Two dimensional numerical and three dimensional analogue modeling, *Geochem. Geophys. Geosyst.*, *5*, Q10003, doi:10.1029/2004GC000748.

Platt, J. P., J.-I. Soto, M. J. Whitehouse, A. J. Hurford, and S. P. Kelley (1998), Thermal evolution, rate of exhumation, and tectonic significance of metamorphic rocks from the floor of Alboran extensional basin, western Mediterranean, *Tectonics*, *17*, 671–689.

Saleeby, J., and Z. Foster (2004), Topographic response to mantle lithosphere removal in the southern Sierra Nevada region, California, *Geology*, *32*, 245–248.

Tackley, P. J., D. J. Stevenson, G. A. Glatzmier, and G. Schubert (1994), Effects of multiple phase transitions in a 3-D spherical model of convection in the Earth's mantle, *J. Geophys. Res.*, *99*, 15,877–15,901.

Zandt, G. (2003), The southern Sierra Nevada drip and the mantle wind direction beneath the southwestern United States, *Int. Geol. Rev.*, *45*, 213–224.

Zandt, G., H. Gilbert, T. J. Owens, M. Ducea, J. Saleeby, and C. H. Jones (2004), Active foundering of a continental arc root beneath the southern Sierra Nevada in California, *Nature*, *432*, 41–46.

————————————
O. H. Göğüş and R. N. Pysklywec, Department of Geology, University of Toronto, 22 Russell Street, Toronto, ON, Canada M5S 3B1. (gogus@geology.utoronto.ca; russ@geology.utoronto.ca)